Inorganic Chemistry

pubs.acs.org/IC Article

High-Pressure, High-Temperature Synthesis and Characterization of Polar and Magnetic $LuCrWO_6$

Sun Woo Kim, Xiaoyan Tan, Corey E. Frank, Zheng Deng, Huaiyu Wang, Liam Collins, Saul H. Lapidus, Changqing Jin, Venkatraman Gopalan, Sergei V. Kalinin, David Walker, and Martha Greenblatt*

Cite This: *Inorg. Chem.* 2020, 59, 3579−3584 Read Online

ACCESS | Metrics & More | Article Recommendations | Supporting Information

ABSTRACT: A new polar and magnetic oxide, $LuCrWO_6$, was synthesized under high pressure (6 GPa) and high temperature (1673 K). $LuCrWO_6$ is isostructural with the previously reported polar $YCrWO_6$ (SG: $Pna2_1$, no. 33). The ordering of CrO_6 and WO_6 octahedra in the edge-shared dimers induce the polar structure. The effective size of rare earth, Ln cation does not seem to affect the symmetry of $LnCrWO_6$. Second harmonic generation measurements of $LuCrWO_6$ confirmed the noncentrosymmetric character and strong piezoelectric domains are observed from piezoresponse force microscopy at room temperature. $LuCrWO_6$ exhibits antiferromagnetic behavior, T_N, of ∼18 K with a Weiss temperature of −30.7 K.

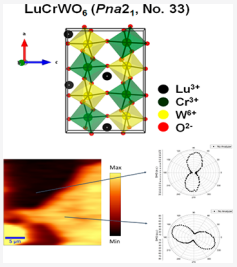

INTRODUCTION

The development of new multifunctional inorganic materials such as multiferroic/magnetoelectric materials has been researched extensively, and various candidate materials have been synthesized and characterized.[1,2] In order to have these properties, the materials should crystallize in one of ten polar crystal classes, i.e., 1, 2, 3, 4, 6, *m*, *mm*2, 3*m*, 4*mm*, or 6*mm*, as well as have magnetic behavior. A number of strategies have been developed for the design of new multifunctional materials; for example, (1) the modification of magnetic cations in a polar $LiNibO_3$-type or Ni_3TeO_6-type and others[3−7] and (2) the combination of second-order Jahn−Teller distortions and/or lone pair cations (Pb^{2+}, Bi^{3+}, Se^{4+}, Te^{4+}, I^{5+}) with magnetic cations.[8−12] However, designing new polar and magnetic oxide materials with better properties is still challenging.

We have focused on finding new structure types to demonstrate breaking the inversion symmetry by cation ordering/rearrangement to discover new multifunctional materials. Our earlier study of $PbSb_2O_6$-related ($ABB'O_6$) and $CaTa_2O_6$-related (aeschynite-type $LnBB'O_6$) materials established that by ordering, or rearranging of the B/B′ cations, the inversion symmetry of the parent compound could be broken. For example, $PbMnTeO_6$ ($P\bar{3}1m$, no. 162 → $P\bar{6}2m$, no. 189),[13] A(II)$GeTeO_6$ (A = Mn, Cd, and Pb) ($P\bar{3}1m$, no. 162 → $P312$, no. 149)[14] and $YCrWO_6$ (*Pnma*, no. 62 → $Pna2_1$, no. 33).[12]

Ordered aeschynite-type $LnMWO_6$ (M = Cr, Fe) materials have been investigated with possible multiferroic behavior.[10−12] For example, $LnFeWO_6$ (Ln = Dy, Eu, Tb, and Y) showed magnetoelectric multiferroicity.[10] Interestingly, Thorogood et al., reported structural changes in $Ln(Ti^{4+}Ta^{5+})O_6$ materials attributable to the size of Ln cation (aeschynite-type, *Pnma*, no. 62 to euxenite-type, *Pbcn*, no. 61).[15] These results suggested that the symmetry of $LnCrWO_6$ will be also changed by the size of the Ln cation. This was our motivation to find new multifunctional oxide materials with ordered aeschynite-type $LnMWO_6$ through exploratory synthesis. Here, we report the high-pressure and high-temperature synthesis and investigation of crystal structure−property relationships of a new polar and magnetic oxide, $LuCrWO_6$.

EXPERIMENTAL SECTION

Reagents. Lu_2O_3 (Alfa Aesar, 99.99%), Cr_2O_3 (Alfa Aesar, 99.97%), and WO_3 (Alfa Aesar, 99.8%) were used without any further purification.

Synthesis. Polycrystalline $LuCrWO_6$ was prepared by a high-pressure and high-temperature synthesis in a Walker-type Multi-Anvil press, as described in our previous work.[5,7,16−20] Stoichiometric amounts of Lu_2O_3, Cr_2O_3, and WO_3 were first ground well at ambient pressure. The oxide mixture was then packed into a Pt capsule inside a MgO crucible, which was later assembled with other parts of the high-pressure apparatus. The reaction was carried out at 1673 K under 6 GPa for 0.5 h and then quenched to about 400 K in a few seconds and 300 K in a few minutes. After quenching, the pressure was slowly released. The resulting sample was a black pellet with a total mass of ∼25 mg.

Laboratory and Synchrotron Powder X-ray Diffraction. $LuCrWO_6$ was characterized by powder X-ray diffraction (PXRD, Bruker-AXS D8-Advanced diffractometer with Cu $K\alpha_1$, λ = 1.5406 Å, 40 kV, 40 mA) for purity and phase identification. Synchrotron powder X-ray diffraction (SPXD) data were collected at 11-BM

Received: September 29, 2019
Published: February 26, 2020

https://dx.doi.org/10.1021/acs.inorgchem.9b02900
Inorg. Chem. 2020, 59, 3579−3584

beamline of the Advanced Photon Source (APS), Argonne National Laboratory, with X-ray wavelength λ = 0.414577 Å. Diffraction data analysis and Rietveld refinement were performed with the TOPAS[21] and GSAS-EXPGUI[22] software package based on the previously reported single crystal data of $YCrWO_6$.[12]

Second Harmonic Generation (SHG). Temperature dependence of optical SHG of $LuCrWO_6$ was obtained by measurements of pellets in a reflection geometry at normal incidence, with an 800 ± 5 nm fundamental input generated by a Ti-sapphire laser (Spectra-Physics, 100 fs pulses, 1 kHz frequency). The SHG signal was detected with a photomultiplier tube (Hamamatsu H7926). The samples were heated to 800 °C and cooled at a rate of 10.0 °C/min on a home-built heating stage.

Scanning Probe Microscopy (SPM). Nanoscale characterization was performed using dual amplitude resonance tracking ((DART)-PFM)[23] and contact Kelvin probe force microscopy (cKPFM).[24] All measurements were performed with a commercial AFM (Cypher ES, Asylum Research and Oxford Instruments Company) equipped with a conductive Budgetsensor Multimode probe (nominal force constant = 3 N/m, nominal resonance frequency = 75 kHz). Generation of the excitation signal and data acquisition were performed with a National Instrument DAQ card and chassis, interfaced with LabView programs. For AC excitation, a signal of 8 V and a frequency centered around the contact resonance were applied. The obtained response was fitted using a simple harmonic oscillator model to extract the amplitude, phase, resonance frequency, and Q-factor. Data processing and analysis were partially performed using pycroscopy.[25]

Magnetic Measurements. The magnetic measurements of $LuCrWO_6$ were performed with a commercial Quantum Design SQUID VSM Magnetometer. The DC magnetic susceptibility data were collected between $2 \leq T \leq 300$ K under an applied magnetic field of 1000 Oe. Isothermal magnetization curves were obtained for magnetic fields: $-7\ T \leq H \leq 7\ T$ at T = 5 and 300 K.

RESULTS AND DISCUSSION

Synthesis. Previously, Thorogood et al., reported that for $Ln(Ti^{4+}Ta^{5+})O_6$ the larger Ln cations (La–Dy) formed an aeschynite-type structure ($CaTa_2O_6$-related, *Pnma*, no. 62) and the smaller Ln cation (Ho–Lu) formed euxenite ($CaNb_2O_6$-related, *Pbcn*, no. 61) structure.[15] We selected one of the smallest Ln cations, Lu^{3+}, to observe a possible structural transformation in $LnCrWO_6$, as seen in $Ln(Ti^{4+}Ta^{5+})O_6$ as a function of the size of the Ln ion. We were unable to synthesize $LuCrWO_6$ with synthetic conditions similar to those previously reported for $YCrWO_6$ (1423 K for 12 h at 1 atm). $Lu(TiTa)O_6$ was synthesized at 1773 K for 12 h by Thorogood et al., who suggested that a higher temperature and longer reaction time will help form a pure and dense sample; however, at a high temperature, rare earth cations can be lost.[15] Therefore, we carried out our reaction under high temperature and high pressure (1673 K under 6 GPa), because a shorter reaction time (30 min) could be used than that required at ambient pressure. It is noteworthy that, comparing the volume of the $LuCrWO_6$ product (60.58 cc/mol) formed at the high temperature and pressure with those of the reagents used for the reaction (68.06 cc/mol), it is evident that the higher pressure thermodynamically favored the smaller volume of the product. Therefore, the high-pressure synthetic condition used was critical for the formation of a stable $LuCrWO_6$ product.

Structure. The structural refinements for $LuCrWO_6$ were performed on SPXD data based on the $YCrWO_6$ structural model ($Pna2_1$, no. 33).[12] From the Rietveld refinement, R_p = 5.71%, R_{wp} = 8.49%, and χ^2 = 2.41 with lattice parameter of a = 10.86444(1) Å, b = 5.09979(1) Å, c = 7.26333(1) Å, where $\alpha = \beta = \gamma = 90°$, V = 402.435(1) (Å)^3, and Z = 4. All atoms are located at 4*a* (x, y, z) positions in $Pna2_1$. The Rietveld refinement plot of PXRD data for $LuCrWO_6$ is shown in Figure 1; crystallographic information, atomic coordinates and

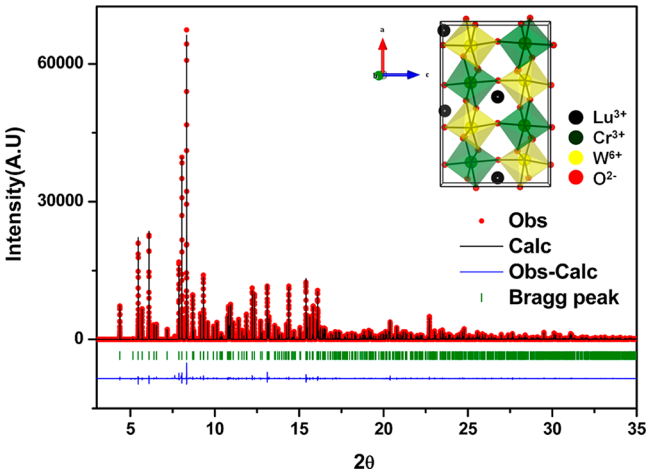

Figure 1. Rietveld refinement plot from Synchrotron XRD data for $LuCrWO_6$. Inset shows crystal structure of $LuCrWO_6$ in the *ac*-plane.

Table 1. Crystallographic Data of $LuCrWO_6$

source	synchrotron
chemical formula	$LuCrWO_6$
formula weight (g/mol)	506.81
temperature (K)	300
wavelength	λ = 0.41458 Å
crystal system	orthorhombic
space group	$Pna2_1$ (no. 33)
unit cell dimensions	a = 10.86444(1) Å, b = 5.09979(1) Å, c = 7.26333(1) Å; $\alpha = \beta = \gamma = 90°$
volume (Å^3)	402.435(1)
Z	4
density (calculated) (g/cm^3)	8.365
χ^2, R_p, R_{wp}	2.41, 5.71, 8.49

atomic displacement parameters are summarized in Table 1 and 2, respectively. Compared to the volume of reported for isostructural compounds, $YCrWO_6$ (410.02(5) Å^3)[12] and $DyCrWO_6$ (412.836(1) Å^3),[11] $LuCrWO_6$ has a smaller volume (402.435(1) Å^3), which is attributable to the smaller effective ionic radius of Lu^{3+}(0.977 Å) compared to those of Y^{3+} (1.019 Å) and Dy^{3+} (1.027 Å), respectively.

The crystal structure of $LuCrWO_6$ consists of $Cr(1)O_6$ and $W(1)O_6$ octahedra, which form edge-sharing dimers; these dimers are linked by corner sharing to form a three-dimensional framework structure. Lu^{3+} cations (LuO_8 polyhedra) are located in the framework (see inset of Figure 1). Compared to the parent $CaTa_2O_6$ structure (*Pnma*, no., 62), the ordered arrangement of Cr^{3+} and W^{6+} cation in the edge-shared dimers induces the polar structure. The origin of such ordering is due to the difference of the octahedral distortion between CrO_6 and WO_6 (distortion parameter, $\Delta d \times 10^{-3}$ = 0.277 for Cr^{3+} and 2.38 for W^{6+}, respectively), which is attributed to the Coulombic repulsion of Cr^{3+}/W^{6+} off-centered position in the edge-sharing octahedra and the second-order Jahn–Teller (SOJT) effect of WO_6 octahedra.

https://dx.doi.org/10.1021/acs.inorgchem.9b02900
Inorg. Chem. 2020, 59, 3579–3584

Table 2. Unit Cell Parameter, Atomic Coordinates, and Displacement Parameter for $LuCrWO_6$[a]

atom	Wyck.	*x*	*y*	*z*	U_{iso} (Å^2)
Lu(1)	4*a*	0.54349(1)	0.95517(1)	0.52026(1)	0.00427(1)
Cr(1)	4*a*	0.36763(1)	0.54791(1)	0.76892(1)	0.00315(1)
W(1)	4*a*	0.35315(1)	0.55732(1)	0.27589(1)	0.00332(1)
O(1)	4*a*	0.38204(1)	0.67708(1)	0.52166(1)	0.00445(1)
O(2)	4*a*	0.21429(1)	0.38435(1)	0.33865(1)	0.00415(1)
O(3)	4*a*	0.29298(1)	0.88154(1)	0.20568(1)	0.00455(1)
O(4)	4*a*	0.52669(1)	0.73644(1)	0.81764(1)	0.00395(1)
O(5)	4*a*	0.35517(1)	0.43871(1)	0.02555(1)	0.00545(1)
O(6)	4*a*	0.47905(1)	0.25413(1)	0.73087(1)	0.00385(1)

[a]From SPXD Rietveld refinement using SG $Pna2_1$ (no. 33). R_p = 5.71%, R_{wp} = 8.49%, and χ^2 = 2.41. Unit cell: *a* = 10.86444(1) Å, *b* = 5.09979(1) Å, *c* = 7.26333(1) Å; $\alpha = \beta = \gamma = 90°$, *V* = 402.435(1) (Å)^3, and *Z* = 4.

Compared with the distortion parameters in $YCrWO_6$ ($\Delta d \times 10^{-3}$ = 0.108 for Cr^{3+} and 2.70 for W^{6+}, respectively),[12] the distortion of CrO_6 increased and the distortion of WO_6 decreased in $LuCrWO_6$. In $LuCrWO_6$, the Cr−O bond distances range between 1.919(3) and 2.009(1) Å, 1.806(1) and 2.086(9) Å for those of W−O, and 2.284(9) and 2.419(3) Å for those of Lu−O. The bond angles of Cr−O−W range between 99.5(7)° and 144.8(4)°. Selected bond distances and angles for $LuCrWO_6$ are summarized in the Table 3. Bond valence sum calculations[26,27] resulted in values of 3.16, 3.03, and 6.12 for Lu^{3+}, Cr^{3+}, and W^{6+}, respectively (See Table 3).

We expected that the small Ln cation, Lu^{3+}, would affect the crystal symmetry of $LuCrWO_6$; however, no structural change comparable to that observed in $Ln(Ti^{4+}Ta^{5+})O_6$ (Ln = La, Ce, Pr, Nd, Sm, Eu, Gd, Tb, Dy, Ho, Er, Tm, Yb, and Lu)[15] was seen. This result indicates that the ordering of Cr^{3+} and W^{6+} in $LuCrWO_6$ is the important factor to determine the structure symmetry, and the size of Ln cation may not have a significant effect on the $LnCrWO_6$ structure.

Table 3. Selected Bond Distances, Angles, and Bond Valences Sum for $LuCrWO_6$

cation	anion	bond length (Å)	BVS
Lu(1)	O(1)	2.255(7)	3.01 (Lu^{3+})
	O(2)	2.419(3)	
	O(3)	2.379(9)	
	O(4)	2.284(9)	
	O(4)	2.437(8)	
	O(5)	2.291(1)	
	O(6)	2.270(4)	
	O(6)	2.370(1)	
Cr(1)	O(1)	1.919(3)	3.10 (Cr^{3+})
	O(2)	1.998(1)	
	O(3)	1.993(9)	
	O(4)	2.009(1)	
	O(5)	1.950(1)	
	O(6)	1.945(9)	
W(1)	O(1)	1.912(6)	6.04 (W^{6+})
	O(2)	1.806(1)	
	O(3)	1.849(7)	
	O(4)	2.010(1)	
	O(5)	1.916(4)	
	O(6)	2.086(9)	
		angle (deg)	
Cr(1)−O(1)−W(1)		138.6(2)	
Cr(1)−O(2)−W(1)		136.6(7)	
Cr(1)−O(3)−W(1)		128.7(6)	
Cr(1)−O(4)−W(1)		100.1(1)	
Cr(1)−O(5)−W(1)		144.8(4)	
Cr(1)−O(6)−W(1)		99.5(7)	

Second Harmonic Generation (SHG). The second harmonic generation of $LuCrWO_6$ was measured to confirm the absence of center of symmetry. In Figure 2a the SHG image shows domain contrast, corroborating a noncentrosymmetric character. We have also investigated the temperature dependence of SHG to gain insight on the origin of the noncentrosymmetric (NCS) property of $LuCrWO_6$ and to explore the possibility of noncentrosymmetric (NCS) -to-centrosymmetric (CS) phase transition.

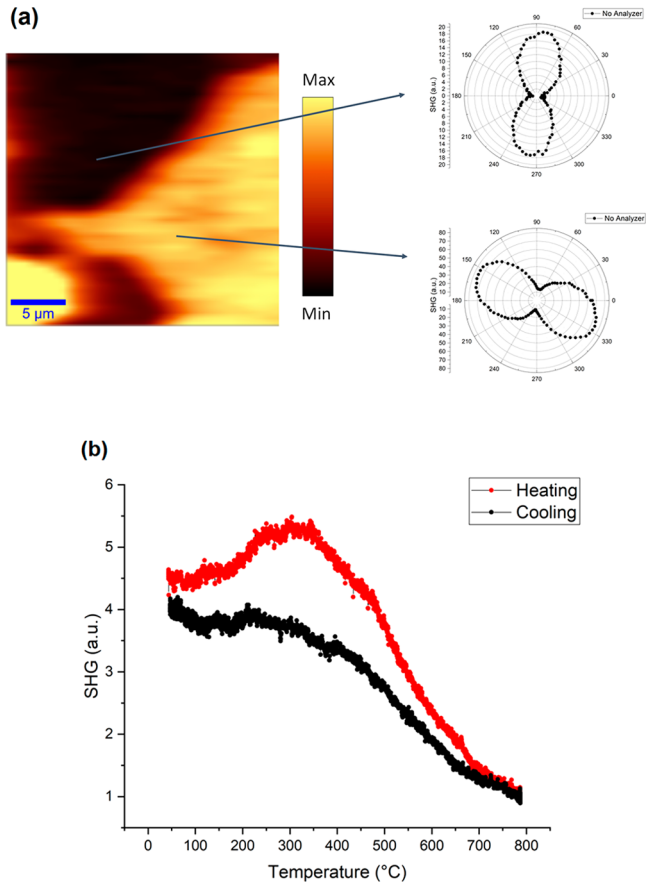

Figure 2. (a) SHG mapping for $LuCrWO_6$ pellet and (b) temperature dependence of optical SHG intensity for $LuCrWO_6$ pellet between 0 and 800 °C.

https://dx.doi.org/10.1021/acs.inorgchem.9b02900
Inorg. Chem. 2020, 59, 3579−3584

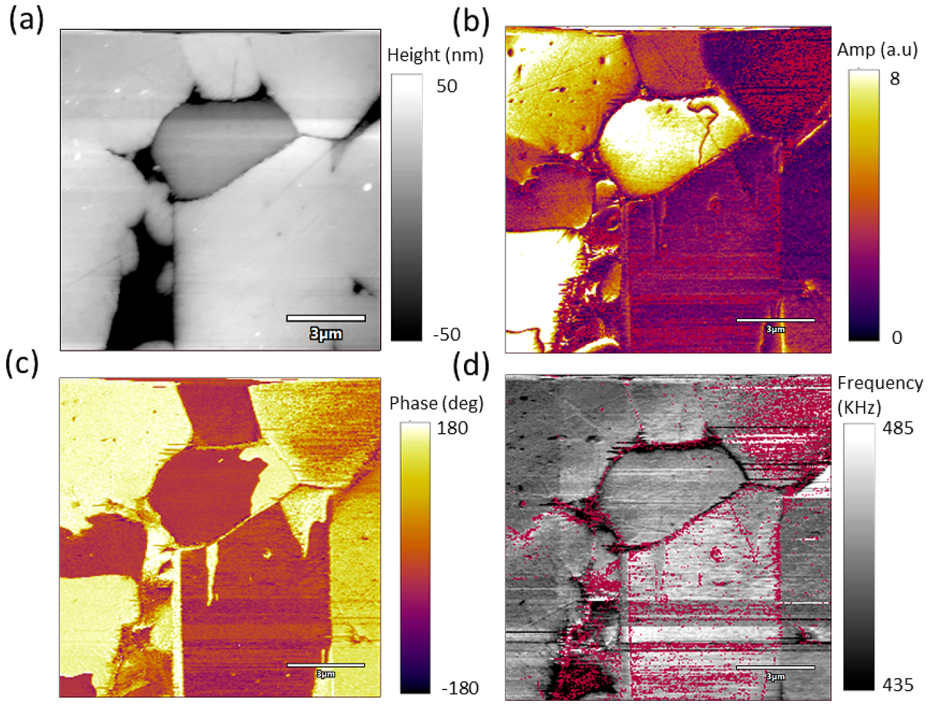

Figure 3. Dart PFM imaging showing (a) height, (b) PFM amplitude, (c) phase, and (d) contact resonance frequency.

In Figure, 2b, the SHG signal as a function of temperature for $LuCrWO_6$ is finite in the whole range of temperature measured; the SHG intensity gradually decreases with increasing temperature, but no NCS-to-CS phase transition is observed. Since NCS was attributed to the ordering of the Cr^{3+} and W^{6+} octahedral cations, the temperature-dependent SHG indicates that as expected, cation ordering decreases with increasing temperature. Note that SHG might saturate at ~300 °C, which would suggest long-range ordering of Cr^{3+} and W^{6+}. The hysteresis in the SHG of the heating and cooling cycles could also be due to a phase transition in this material (Figure 2b).

Piezoresponse Force Microscopy (PFM) and Contact Kelvin Probe Force Microscopy (cKPFM). Piezoresponse force microscopy (PFM) was used to examine the presence of piezoelectrical response in $LuCrWO_6$ at room temperature. AFM topography of the polished sample embedded in epoxy (Figure 3a) shows clear grain structures with a few holes, and the corresponding PFM amplitude image (Figure 3b) indicates strong domain contrast with single grains, which indicates that the material has a strong piezoelectric response. The domains are correlated with phase changes in Figure 3c, showing 180° phase inversion between some domains across the surface. Finally, in Figure 3d, the frequency maps show a stable value, with contrast observed only at the pits, resulting from sudden changes in the tip−sample contact, which effectively demonstrates that the PFM response is real and not an artifact of topography effects. On certain locations (purple pixels) the simple harmonic oscillator (SHO) fit was not robust, and the software automatically discards that pixel data.

Next, the switching properties of the material were examined with contact Kelvin probe force microscopy (cKPFM). We performed cKPFM on a 15 × 15 grid in a similar region to the previous PFM measurement (Figure S1). The mean cKPFM curves over the entire grid is shown in the Supporting Information Figure S1. The cKPFM shows a linear single band structure, indicating that hysteretic polarization switching has not occurred, in which case we would expect to show a double band structure. In conclusion, we observe clear piezoelectric domain contrast with PFM, and although $LuCrWO_6$ may in fact be ferroelectric, ferroelectric switching with cKPFM was not observed.

Magnetic Behavior. In Figure 4a,b the DC magnetic susceptibility, χ and $1/\chi$ versus temperature, respectively, of $LuCrWO_6$, measured under 1000 Oe and 2−300 K, shows three-dimensional magnetic behavior with a sharp Néel transition temperature (T_N) at ~18 K.[28,29]

The ZFC (zero field cooling) and FC (field cooling) magnetization curves overlap, which is consistent with the ordering of the cations. The $1/\chi$ versus temperature data (Figure 4b), were fit to the Curie−Weiss (CW) law, $\chi = C/(T - \theta)$ for T = 50−300 K, where C is the Curie constant and θ is the Weiss constant: C = 2.061 emu K mol^{-1} and θ = −30.69 K were extracted from the CW fit of the data. From the CW fit, the effective magnetic moment, μ_{eff} = 4.06 μ_B/Cr is slightly higher than the theoretical spin only value for Cr^{3+} (3.87 μ_B, S = 3/2). The negative Weiss constant confirms AFM interactions, which are attributed to super−superexchange interaction of long-range chains of Cr^{3+}−O^{2-}−W^{6+}−O^{2-}−Cr^{3+}.[28,29] In Figure S1, the isothermal magnetization of $LuCrWO_6$ measured as a function of applied field H at 5 and 300 K indicates that some degree of spin reorientations is present below T_N (~18 K). $LuCrWO_6$ shows similar magnetic behavior as the previously reported $YCrWO_6$.[12]

CONCLUSION

A new polar and magnetic oxide, $LuCrWO_6$ with a $CaTa_2O_6$-related structure was successfully synthesized with high pressure and high temperature. Due to the ordering of Cr^{3+} and W^{6+} cations in the octahedral environment, $LuCrWO_6$ adopts a lower symmetry polar space group, $Pna2_1$ (no. 33), in contrast to its centrosymmetric ($Pnma$, no. 62) structural

https://dx.doi.org/10.1021/acs.inorgchem.9b02900
Inorg. Chem. 2020, 59, 3579−3584

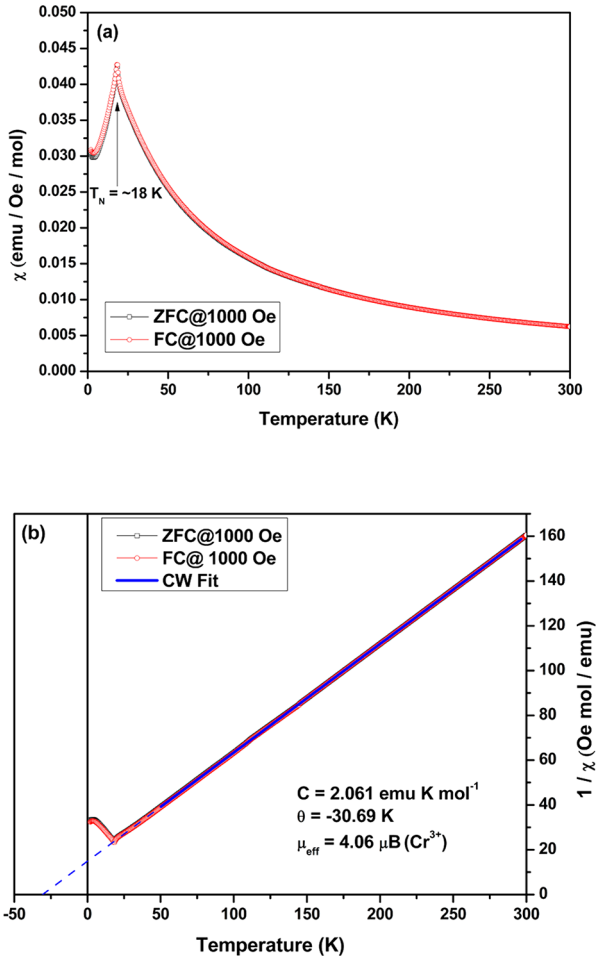

Figure 4. Magnetic susceptibility, χ of $LuCrWO_6$: (a) Temperature dependence of χ measured in 1000 Oe and (b) $1/\chi$ with a Curie–Weiss fit (solid line).

analogue, $CaTa_2O_6$. The size of Ln (e.g., Y, Lu) cations does not appear to affect the symmetry of $LnCrWO_6$. Second harmonic generation of $LuCrWO_6$ confirms noncentrosymmetric character, while PFM measurements show strong piezoelectric domains; however, no clear polarization switching is observed to evidence ferroelectric behavior. $LuCrWO_6$ orders antiferromagnetically at $T_N \sim 18$ K. Further compositional modification studies of a $LnM(III)WO_6$ (M = Mn, Fe, Co, Rh) series are in progress to validate symmetry breaking principles to discover new multiferroic/magnetoelectric materials.

■ ASSOCIATED CONTENT

Supporting Information

The Supporting Information is available free of charge at https://pubs.acs.org/doi/10.1021/acs.inorgchem.9b02900.

Figures of contact resonance KPFM curves and isothermal magnetization (PDF)

Accession Codes

CCDC 1943296 contains the supplementary crystallographic data for this paper. These data can be obtained free of charge via www.ccdc.cam.ac.uk/data_request/cif, or by emailing data_request@ccdc.cam.ac.uk, or by contacting The Cambridge Crystallographic Data Centre, 12 Union Road, Cambridge CB2 1EZ, UK; fax: +44 1223 336033.

■ AUTHOR INFORMATION

Corresponding Author

Martha Greenblatt − *Department of Chemistry and Chemical Biology, Rutgers, the State University of New Jersey, Piscataway, New Jersey 08854, United States;* orcid.org/0000-0002-1806-2766; Email: greenbla@chem.rutgers.edu

Authors

Sun Woo Kim − *Department of Chemistry Education, Chosun University, Gwangju 61452, South Korea; Department of Chemistry and Chemical Biology, Rutgers, the State University of New Jersey, Piscataway, New Jersey 08854, United States;* orcid.org/0000-0003-1057-2283

Xiaoyan Tan − *Department of Chemistry and Chemical Biology, Rutgers, the State University of New Jersey, Piscataway, New Jersey 08854, United States;* orcid.org/0000-0002-1742-8252

Corey E. Frank − *Department of Chemistry and Chemical Biology, Rutgers, the State University of New Jersey, Piscataway, New Jersey 08854, United States*

Zheng Deng − *Beijing National Laboratory for Condensed Matter Physics, Institute of Physics, Chinese Academy of Sciences, Beijing 100190, China*

Huaiyu Wang − *Department of Materials Science and Engineering, Pennsylvania State University, University Park, Pennsylvania 16802, United States*

Liam Collins − *Center for Nanophase Material Science & Institute for Functional Imaging Materials, Oak Ridge National Laboratory, Oak Ridge, Tennessee 37831, United States;* orcid.org/0000-0003-4946-9195

Saul H. Lapidus − *Advanced Photon Source, Argonne National Laboratory, Lemont, Illinois 60439, United States*

Changqing Jin − *Beijing National Laboratory for Condensed Matter Physics, Institute of Physics, Chinese Academy of Sciences, Beijing 100190, China*

Venkatraman Gopalan − *Department of Materials Science and Engineering, Pennsylvania State University, University Park, Pennsylvania 16802, United States;* orcid.org/0000-0001-6866-3677

Sergei V. Kalinin − *Center for Nanophase Material Science & Institute for Functional Imaging Materials, Oak Ridge National Laboratory, Oak Ridge, Tennessee 37831, United States;* orcid.org/0000-0001-5354-6152

David Walker − *Lamont-Doherty Earth Observatory, Columbia University, Palisades, New York 10964, United States*

Complete contact information is available at: https://pubs.acs.org/10.1021/acs.inorgchem.9b02900

Author Contributions

The manuscript was written by contributions of all authors.

Notes

The authors declare no competing financial interest.

■ ACKNOWLEDGMENTS

S.W.K. gratefully acknowledges support from the National Research Foundation of Korea (NRF) funded by the Ministry of Science and ICT (2018R1C1B5085301). The work at Rutgers was supported by the US NSF-DMR-1507252 grant. H.W. and V.G. acknowledge funding from NSF grant DMR-1729338 and the Penn State NSF-MRSEC Center for Nanoscale Science grant no. DMR-1420620. The use of the Advanced Photon Source at the Argonne National Laboratory

https://dx.doi.org/10.1021/acs.inorgchem.9b02900
Inorg. Chem. 2020, 59, 3579−3584

was supported by the U. S. Department of Energy, Office of Science, Office of Basic Sciences, under Contact no. DE-AC02-06CH11357.

REFERENCES

(1) Spaldin, N. A.; Fiebig, M. Materials science: the renaissance of magnetoelectric multiferroics. *Science* **2005**, *309*, 391−392.
(2) Eerenstein, W.; Mathur, N. D.; Scott, J. F. Multiferroic and magnetoelectric materials. *Nature* **2006**, *442*, 759−765.
(3) Li, M.-R.; Walker, D.; Retuerto, M.; Sarkar, T.; Hadermann, J.; Stephens, P. W.; Croft, M.; Ignatov, A.; Grams, C. P.; Hemberger, J.; Nowik, I.; Halasyamani, P. S.; Tran, T. T.; Mukherjee, S.; Dasgupta, T. S.; Greenblatt, M. Polar and Magnetic Mn_2FeMO_6 (M = Nb, Ta) with $LiNbO_3$-type Structure: High-Pressure Synthesis. *Angew. Chem., Int. Ed.* **2013**, *52*, 8406−8410.
(4) Li, M.-R.; Stephens, P. W.; Retuerto, M.; Sarkar, T.; Grams, C. P.; Hemberger, J.; Croft, M. C.; Walker, D.; Greenblatt, M. Designing Polar and Magnetic Oxides: Zn_2FeTaO_6 - in Search of Multiferroics. *J. Am. Chem. Soc.* **2014**, *136*, 8508−8511.
(5) Li, M.-R.; Croft, M.; Stephens, P. W.; Ye, M.; Vanderbilt, D.; Retuerto, M.; Deng, Z.; Grams, C. P.; Hemberger, J.; Hadermann, J.; Li, W.-M.; Jin, C.-Q.; Saouma, F. O.; Jang, J. I.; Akamatsu, H.; Gopalan, V.; Walker, D.; Greenblatt, M. Mn_2FeWO_6: A new Ni_3TeO_6-type polar and magnetic oxide. *Adv. Mater.* **2015**, *27*, 2177−81.
(6) Fujita, K.; Kawamoto, T.; Yamada, I.; Hernandez, O.; Hayashi, N.; Akamatsu, H.; Lafargue-Dit-Hauret, W.; Rocquefelte, X.; Fukuzumi, M.; Manuel, P.; Studer, A. J.; Knee, C. S.; Tanaka, K. $LiNbO_3$-Type $InFeO_3$: Room-Temperature Polar Magnet without Second-Order Jahn-Teller Active Ions. *Chem. Mater.* **2016**, *28*, 6644−6655.
(7) Li, M.-R.; McCabe, E. E.; Stephens, P. W.; Croft, M.; Collins, L.; Kalinin, S. V.; Deng, Z.; Retuerto, M.; Sen Gupta, A.; Padmanabhan, H.; Gopalan, V.; Grams, C. P.; Hemberger, J.; Orlandi, F.; Manuel, P.; Li, W.-M.; Jin, C.-Q.; Walker, D.; Greenblatt, M. Magnetostriction-polarization coupling in multiferroic Mn_2MnWO_6. *Nat. Commun.* **2017**, *8*, 1−9.
(8) Baettig, P.; Seshadri, R.; Spaldin, N. A. Anti-Polarity in Ideal $BiMnO_3$. *J. Am. Chem. Soc.* **2007**, *129*, 9854−9855.
(9) Retuerto, M.; Li, M. R.; Ignatov, A.; Croft, M.; Ramanujachary, K. V.; Chi, S.; Hodges, J. P.; Dachraoui, W.; Hadermann, J.; Tran, T. T.; Halasyamani, P. S.; Grams, C. P.; Hemberger, J.; Greenblatt, M. Polar and Magnetic Layered A Site and Rock Salt B Site-Ordered $NaLnFeWO_6$ (Ln = La, Nd) Perovskites. *Inorg. Chem.* **2013**, *52*, 12482−12491.
(10) Ghara, S.; Suard, E.; Fauth, F.; Tran, T. T.; Halasyamani, P. S.; Iyo, A.; Rodríguez-Carvajal, J.; Sundaresan, A. Ordered aeschynite-type polar magnets $RFeWO_6$ (R = Dy, Eu, Tb and Y): A new family of type-II multiferroics. *Phys. Rev. B: Condens. Matter Mater. Phys.* **2017**, *95* (22), 224416.
(11) Ghara, S.; Fauth, F.; Suard, E.; Rodriquez-Carvajal, J.; Sundaresan, A. Synthesis, Structure, and Physical Properties of the Polar Magnet $DyCrWO_6$. *Inorg. Chem.* **2018**, *57*, 12827−12835.
(12) Kim, S. W.; Emge, T. J.; Deng, Z.; Uppuluri, R.; Collins, L.; Lapidus, S. H.; Segre, C. U.; Croft, M.; Jin, C.; Gopalan, V.; Kalinin, S. V.; Greenblatt, M. $YCrWO_6$: Polar and Magnetic Oxide with $CaTa_2O_6$-Related Structure. *Chem. Mater.* **2018**, *30*, 1045−1054.
(13) Kim, S. W.; Deng, Z.; Li, M.-R.; Sen Gupta, A.; Akamatsu, H.; Gopalan, V.; Greenblatt, M. $PbMn(IV)TeO_6$: A New Noncentrosymmetric Layered Honeycomb Magnetic Oxide. *Inorg. Chem.* **2016**, *55*, 1333−1338.
(14) Kim, S. W.; Deng, Z.; Yu, S.; Padmanabhan, H.; Zhang, W.; Gopalan, V.; Jin, C.; Greenblatt, M. $A(II)GeTeO_6$ (A = Mn, Cd, Pb): Non-Centrosymmetric Layered Tellurates with $PbSb_2O_6$-Related Structure. *Inorg. Chem.* **2017**, *56*, 9019−9024.
(15) Thorogood, G. J.; Avdeev, M.; Kennedy, B. J. Structural studies of the aeschynite-euxenite transformation in the series $Ln(TiTa)O_6$ Ln = Lanthanide. *Solid State Sci.* **2010**, *12*, 1263−1269.
(16) Li, M.-R.; Hodges, J. P.; Retuerto, M.; Deng, Z.; Stephens, P. W.; Croft, M. C.; Deng, X.; Kotliar, G.; Sanchez-Benitez, J.; Walker, D.; Greenblatt, M. Mn_2MnReO_6: Synthesis and Magnetic Structure Determination of a New Transition-Metal-Only Double Perovskite Canted Antiferromagnet. *Chem. Mater.* **2016**, *28*, 3148−3158.
(17) Li, M.-R.; Stephens, P. W.; Croft, M.; Deng, Z.; Li, W.; Jin, C.; Retuerto, M.; Hodges, J. P.; Frank, C. E.; Wu, M.; Walker, D.; Greenblatt, M. $Mn_2(Fe_{0.8}Mo_{0.2})MoO_6$: A Double Perovskite with Multiple Transition Metal Sublattice Magnetic Effects. *Chem. Mater.* **2018**, *30*, 4508−4514.
(18) Feng, H. L.; Frank, C. E.; Greenblatt, M.; Deng, Z.; Jin, C.; Wu, M.; Li, M.-R.; Croft, M.; Lapidus, S. H.; Liu, S.; Tyson, T. A.; Ravel, B. D.; Quackenbush, N. F.; Walker, D. High-Pressure Synthesis of Lu_2NiIrO_6 with Ferrimagnetism and Large Coercivity. *Inorg. Chem.* **2019**, *58*, 397−404.
(19) Frank, C. E.; McCabe, E. E.; Orlandi, F.; Manuel, P.; Tan, X.; Deng, Z.; Croft, M.; Cascos, V.; Emge, T.; Feng, H. L.; Lapidus, S.; Jin, C.; Wu, M.; Li, M. R.; Ehrlich, S.; Khalid, S.; Quackenbush, N.; Yu, S.; Walker, D.; Greenblatt, M. Mn_2CoReO_6: a robust multi-sublattice antiferromagnetic perovskite with small A-site cations. *Chem. Commun.* **2019**, *55*, 3331−3334.
(20) Tan, X.; McCabe, E. E.; Orlandi, F.; Manuel, P.; Batuk, M.; Hadermann, J.; Deng, Z.; Jin, C.; Nowik, I.; Herber, R.; Segre, C. U.; Liu, S.; Croft, M.; Kang, C.-J.; Lapidus, S.; Frank, C. E.; Padmanabhan, H.; Gopalan, V.; Wu, M.; Li, M.-R.; Kotliar, G.; Walker, D.; Greenblatt, M. $MnFe_{0.5}Ru_{0.5}O_3$: Above-room-temperature antiferromagnetic semiconductor. *J. Mater. Chem. C* **2019**, *7*, 509−522.
(21) Coelho, A. A. Indexing of powder diffraction patterns by iterative use of singular value decomposition. *J. Appl. Crystallogr.* **2003**, *36*, 86−95.
(22) Toby, B. H. EXPGUI, a graphical user interface for GSAS. *J. Appl. Crystallogr.* **2001**, *34*, 210−213.
(23) Jesse, S.; Kalinin, S. V.; Proksch, R.; Baddorf, A. P.; Rodriguez, B. J. The band excitation method in scanning probe microscopy for rapid mapping of energy dissipation on the nanoscale. *Nanotechnology* **2007**, *18*, 435503−435503.
(24) Balke, N.; Maksymovych, P.; Jesse, S.; Herklotz, A.; Tselev, A.; Eom, C.-B.; Kravchenko, I. I.; Yu, P.; Kalinin, S. V. Differentiating Ferroelectric and Nonferroelectric Electromechanical Effects with Scanning Probe Microscopy. *ACS Nano* **2015**, *9*, 6484−6492.
(25) Somnath, S.; Smith, C. R.; Laanait, N.; Vasudevan, R. K.; Ievlev, A.; Belianinov, A.; Lupini, A. R.; Shankar, M.; Kalinin, S. V.; Jesse, S. USID and pycroscopy - open frameworks for storing and analyzing spectroscopic and imaging data. *Microsc. Microanal.* **2019**, *25*, 1−33.
(26) Brown, I. D.; Altermatt, D. Bond-valence parameters obtained from a systematic analysis of the inorganic crystal structure database. *Acta Crystallogr., Sect. B: Struct. Sci.* **1985**, *B41*, 244−247.
(27) Brown, I. D. Recent Developments in the Methods and Applications of the Bond Valence Model. *Chem. Rev.* **2009**, *109*, 6858−6919.
(28) Whangbo, M.-H.; Koo, H.-J.; Dai, D. Spin exchange interactions and magnetic structures of extended magnetic solids with localized spins: theoretical descriptions on formal, quantitative and qualitative levels. *J. Solid State Chem.* **2003**, *176*, 417−481.
(29) Xiang, H.; Lee, C.; Koo, H.-J.; Gong, X.; Whangbo, M.-H. Magnetic properties and energy-mapping analysis. *Dalton Trans.* **2013**, *42*, 823−853.

https://dx.doi.org/10.1021/acs.inorgchem.9b02900
Inorg. Chem. 2020, 59, 3579−3584